Published in final edited form as:
J Comp Neurol. 2014 December 1; 522(14): 3141–3159. doi:10.1002/cne.23625.

Large basolateral processes on type II hair cells comprise a novel processing unit in mammalian vestibular organs

Rémy Pujol[1,2], **Sarah B. Pickett**[2], **Tot Bui Nguyen**[2], and **Jennifer S. Stone**[2]

[1]INSERM Unit 1051, Institute of Neuroscience, Montpelier, France

[2]The Virginia Merrill Bloedel Hearing Research Center, and the Department of Otolaryngology-Head and Neck Surgery, University of Washington, Seattle, WA

Abstract

Sensory receptors in the vestibular system (hair cells) encode head movements and drive central motor reflexes that control gaze, body movements, and body orientation. In mammals, type I and II vestibular hair cells are defined by their shape, contacts with vestibular afferent nerves, and membrane conductance. Here, we describe unique morphological features of type II vestibular hair cells in mature rodents (mice and gerbils) and bats. These features are cytoplasmic processes that extend laterally from the hair cell's base and project under type I hair cells. Closer analysis of adult mouse utricles demonstrated that the basolateral processes of type II hair cells range in shape, size, and branching, with the longest processes extending 3–4 hair cell widths. The hair cell basolateral processes synapse upon vestibular afferent nerves and receive inputs from vestibular efferent nerves. Further, some basolateral processes make physical contacts with the processes of other type II hair cells, forming some sort of network amongst type II hair cells. Basolateral processes are rare in perinatal mice and do not attain their mature form until 3–6 weeks of age. These observations demonstrate that basolateral processes are significant signaling regions of type II vestibular hair cells, and they suggest type II hair cells may directly communicate with each other, which has not been described in vertebrates.

Corresponding Author: Jennifer S. Stone, Ph.D., CHDD CD176 Box 357923, Virginia Merrill Bloedel Hearing Research Center, Department of Otolaryngology—Head and Neck Surgery, University of Washington, Seattle, WA 98195-7923, Phone: 206-616-4108, Fax: 206-221-5685, stoner@u.washington.edu.

CONFLICT OF INTEREST STATEMENT

None of the authors of this paper have current or potential conflicts of interest that have influenced the content of this paper.

ROLES OF AUTHORS

Rémy Pujol was a visiting scientist at the Virginia Merrill Bloedel Hearing Research Center. During this time, he helped the Stone lab to execute TEM analyses of adult mouse utricles. Rémy was instrumental in defining the positions and shapes of type II hair cell basolateral processes and in examining their contacts with afferent and efferent nerves, and with other processes.

Sarah Pickett is a graduate student in the Neurobiology and Behavior Program. During her three-month rotation in the Stone lab in the fall of 2012, Sarah characterized the shape of the basolateral processes over the course of postnatal development. She performed segmentations and measurements of the processes. She prepared the quantitative data and performed statistical analyses.

Tot Bui Nguyen is a research scientist in the Stone lab. She prepared most of the animal samples for this project. This included tissue fixation, dissection, immunolabeling, embedding, and sectioning. Tot also performed over half of the confocal imaging for the project.

Jennifer Stone conceived of the project and recruited Rémy Pujol's participation. Jenny managed the work of all individuals involved in the project. She also performed a significant portion of the confocal imaging. Jenny constructed all of the figures and she wrote most of the text for the paper.

Keywords

Vestibular; type II hair cell; morphology; mammal; synapse; JAX:000654; JAX:000664; RGD: 737903; AB_10013626; AB_10015251; AB_2282417; AB_2068506; AB_2068336; AB_477329; AB_177520; AB_10175616; AB_2113875; AB_399431; AB_2079751; AB_2286684

INTRODUCTION

In mammals, five vestibular organs in the inner ear encode movements of the head and thereby regulate gaze, body movements, and body orientation. The saccule and utricle have a flat sensory epithelium called a macula, and they respond to linear head acceleration and head tilt. The anterior, posterior, and lateral ampullae have a more complexly shaped sensory epithelium called a crista, and they detect head rotation in a range of planes.

Hair cells are the sensory mechanoreceptors in these organs. Directional deflections of long microvilli (stereocilia) on the surfaces of hair cells drive action potentials in eighth cranial (vestibular) nerve afferents, which leads to neuronal activity in several brain regions. Amniotes have two types of vestibular hair cells: I and II. In rodents, the two hair cell types are present in similar numbers, and they are found in all zones of the vestibular sensory epithelium (Desai et al., 2005; Kirkegaard and Nyengaard, 2005). However, type I and II hair cells are distinct in many respects (reviewed in Eatock and Songer, 2011), including shape (e.g., Wersäll, 1956; Lysakowski and Goldberg, 1997), molecular profile (e.g., Dechesne et al., 1991; Sans et al., 2001; Desai et al., 2005; Oesterle et al., 2008), bundle morphology (Lapeyre et al., 1982; Peterson et al., 1996; Li et al., 2008), membrane properties (Correia and Lang, 1990; Rennie and Correia, 1994; Ricci et al., 1996; Rüsch and Eatock, 1996), and innervation (e.g., Wersäll, 1956; Fernandez et al., 1988). For example, type I hair cells have been described as flask-shaped and are wrapped by specialized afferent nerve endings called calyces. By contrast, type II hair cells can be cylindrical, goblet-like, or dumb-bell shaped and are contacted by bouton-only afferents (e.g., Lysakowski and Goldberg, 1997). Further, in mature mice and rats, antibodies to the calcium-binding protein calretinin preferentially label type II hair cells in all regions of the vestibular organs (Dechesne et al., 1991; Desai et al., 2005).

Although many features of vestibular hair cells are well defined, we do not understand precisely how each hair cell type contributes to peripheral processing of head movements. In mammals, most vestibular afferents are dimorphic; they have both bouton and calyx endings and therefore contact both type I and type II hair cells (Fernandez et al., 1988). Therefore, vestibular afferent nerve activity is not simply dictated by hair cell type. Properties of hair cells and afferent neurons do correlate strongly with their position in the vestibular epithelium (reviewed in Peterson, 1998; Goldberg, 2000; Eatock and Songer, 2011). For instance, calyx-only afferents are confined to the striolar zone of the macula and the central zone of the crista. By contrast, bouton-only afferents are only found in the extrastriolar zone of the macula and the peripheral zone of the crista. Further, afferents from the striolar or central zone have irregular activity at rest and are fast-adapting, while afferents derived from the extrastriolar or the peripheral zone have regular activity at rest and are non-adapting. At

this point, the mechanisms that shape these spatial differences in afferent activity are also not understood.

Studies of hair cell regeneration in mature rodents suggest type II hair cells may be the predominant cell type that is regenerated in the utricles of adult guinea pigs and mice when both type I and II hair cells are destroyed (Forge et al., 1998; Kawamoto et al., 2009; Golub et al., 2012). Further, all regenerated type II hair cells have an unusual morphology: two or more cytoplasmic processes that emanate from below the nucleus and have elaborate branches (Golub et al., 2012). This morphology is conserved in regenerated hair cells half a year after damage, suggesting it is stable. Cells with basolateral processes have pre-synaptic specializations, and they rapidly take up the styryl dye FM1-43, further supporting the interpretation that type II hair cells with processes are well differentiated and mature. This finding raised the question of whether basolateral processes are normal features of type II hair cells or an abnormal feature of regenerated hair cells. We addressed this question in this study by examining the morphology of type II hair cells in the vestibular epithelia of normal (undamaged) adult mice and other rodents.

MATERIALS AND METHODS

Animals

Experiments in this study used mice (*Mus musculus)*, gerbils (*Meriones unguiculatus*), rats (*Rattus norvegicus*), and bats (*Eptesicus fuscus*). We used CBA/CAJ mice (RRID: JAX: 000654), C57Bl/6J mice (RRID: JAX:000664), and Swiss Webster mice. Mice were purchased from The Jackson Labs (Bar Harbor, ME), Harlan Labs (Indianapolis, IN), or bred at the University of Washington (UW) Animal Facility. All mice used in experiments were post-natal, between 7 and 325 days of age. Mice were considered to be adults if they were 6 weeks of age or older. Both male and female mice were studied. Female adult Mongolian gerbils (strain 243 Crl:MON/Tum) were purchased from Charles River Laboratories (Wilmington, MA). The exact age of the gerbils is unknown, but all females were dams and therefore sexually mature. Male Sprague Dawley rats (RGD: 737903) were purchased from Harlan Laboratories (Indianapolis, IN) and were examined around 40 days of age. Adult big brown bats were bred at the University of Washington, and utricles were examined in bats greater than 56 days of age.

All animal procedures were approved by the University of Washington's Institutional Animal Care and Use Committee and met standards of both the American Veterinary Medical Association and the National Institutes of Health. Mice were euthanized by decapitation after either CO_2 anesthesia (for preparation of fixed tissues) or cervical dislocation (for FM1-43 labeling in organ cultures). Rats and gerbils were euthanized by CO_2 overdose followed by decapitation. Adult bats were killed by pentobarbital overdose followed by transcardial perfusion with fixative.

Organ dissection

After euthanasia, temporal bones from mice, rats, and gerbils were dissected and fixed in 4% buffered paraformaldehyde for 30 min to 2 hours at room temperature. Organs were rinsed

with phosphate-buffered saline (PBS) for several hours. Vestibular end organs (utricles, saccules, and lateral ampullae) were dissected from fixed temporal bones using fine microforceps. In PBS, the structures overlying vestibular organs (otoconia and otoconial membrane) were removed from utricles and saccules using a stream of PBS from a 26-gauge needle or an eyelash glued to a small stick.

Vibratome sectioning

Fixed utricles from adult CBA/CaJ mice, with otoconia removed, were embedded in low-melting point 3.5% agarose (Sigma-Aldrich), dissolved in PBS, and sectioned at 60–80 μm using a vibratome (Leica VT1000S).

Organ immunolabeling

Proteins were detected in whole-mount organs or vibratome sections using standard immunofluorescence labeling methods. Tissue was incubated for 30 min in blocking solution (2% bovine serum albumin, 0.8% normal goat serum, 0.5% Triton X-100 for myosin VIIa detection, or 0.5% Triton-X 100 in PBS with 5% normal serum for detection of other antigens). Tissue was incubated overnight at 4°C with primary antibodies in blocking solution. Table 1 describes the manufacturer, the specificity, and the concentrations of antibodies used in this study. These antibodies were used as cellular markers, and the vast majority of them have been used previously to detect antigens in mouse inner ear sensory epithelia.

Secondary antibodies, conjugated to Alexa 488, 594, or 647 and diluted 1/300, were purchased from Invitrogen (Carlsbad, CA). To label filamentous actin, organs were soaked in phalloidin conjugated to Alexa 488 (Invitrogen) at 10 μg/ml dissolved in PBS containing 0.5% TritonX100. To label cell nuclei, organs were soaked in DAPI (4′,6′-diamidino-2-phenylindole; Sigma-Aldrich) at 1 μg/ml dissolved in PBS for 10 min.

Digital imaging and analysis

Fluorescent images were obtained using an Olympus FV-1000 confocal microscope. For all experiments, Z series images from the lumenal surface of the sensory epithelium through the stroma were obtained using a 20x objective. In some cases, a 60x oil objective was used to take higher-magnification images of regions of interest. For all qualitative analyses, we examined at least 6 organs per variable.

Segmentations of type II hair cells were generated using confocal Z series stacks taken from utricles of adult CBA/CaJ mice that were immunolabeled for calretinin (for Fig. 3) or myosin VIIa (for Fig. 6). Type II hair cells that were either calretinin- or myosin VIIa-positive were selected from confocal stacks, and individual hair cells were segmented using the public domain program Fiji and the Segmentation Editor plug-in, both freely available from http://fiji.sc/ (Schindelin et al., 2012). The cytoplasm from selected cells was manually outlined while stepping through the confocal stack and then filled by manual thresholding. The plug-in placed the filled outline of the cell from each slice into a copy of the stack and optionally interpolated the selection between outlines created in non-adjacent slices. The

stacks containing outlines were treated as individual channels to create merged, multi-color volume renderings to demonstrate hair cell shapes and spatial relationships.

To obtain an estimate of the proportion of hair cells with a particular shape (simple bulbous, complex branched, or intermediate, described in Results, Fig. 3), we counted hair cells with each shape in calretinin-labeled utricles, by scanning offline through Z series collected from the lateral extrastriolar region. We examined 613 calretinin-positive type II hair cells from 4 utricles from adult CBA/CaJ mice.

Measurements of type II hair cell processes at different ages (Fig. 11) were performed as follows. Utricles were dissected from Swiss Webster mice at 4 ages: 7 days, 14 days, 21 days, and adult (>6 weeks). Utricles were immunoreacted with anti-calretinin antibody, as described above, to preferentially label type II hair cells (Dechesne et al., 1991; Desai et al., 2005). For each process, we measured its volume, surface area, and perimeter boundary (the smallest bounding circle that encompassed a two-dimensional brightest point projection of each process). For each measurement, 3 utricles per time point were examined. We selected 30 type II hair cells from each of 3 utricles for each age group. Hair cells were selected for analysis based on our ability to clearly distinguish the extent of the processes and the points of contacts with neighboring hair cells. Z series image stacks (1024 pixel × 1024 pixel) were generated at 60x (oil) from the lateral extrastriolar region only in order to provide consistency across the age groups. Stacks started at the lumenal surface of the epithelium and extended into the stroma; each slice was 0.25 um steps. We used Simple Neurite Tracer (Longair et al., 2011) in the Fiji imaging software (Schindlein et al. 2012) to trace type II hair cell processes. Measurements were taken from the top of the process (just below the nucleus) to the bottom of each process (just above the supporting cell layer). Thus, “processes” were defined as the calretinin-positive cytoplasm deep to the perinuclear cytoplasm.

FM1-43 labeling and measures

Utricles from adult Swiss Webster mice (n=4) were isolated, and otoconia were removed. All steps were performed using pre-warmed (37°C) solutions, and all incubations occurred at 37°C with 95% air/5% CO_2. Utricles were incubated in Hanks buffered saline solution (HBSS) for 5 min followed by HBSS containing 5 mM FM1-43-FX (Invitrogen) for 20 sec. Utricles were rinsed with HBSS two times, incubated in HBSS for 30 more min, and fixed with 4% paraformaldehyde for 30 min. Utricles were then immunolabeled for myosin VIIa to enable us to detect hair cells and imaged using confocal microscopy. In 60x images from 3 fields in two utricles, we estimated the percentage of type II hair cells that had incorporated FM1-43-FX by scoring myosin VIIa-positive hair cells in the type II hair cell layer of Z series stacks as positive or negative for FM1-43-FX signal.

Type I/II hair cell counts

Utricles from adult CBA/CaJ mice (n=2) were immunolabeled for myosin VIIa and counter-labeled with DAPI. Using confocal microscopy and a 60x objective, we generated Z series stacks in 2 extrastriolar and 2 striolar regions from each utricle. Using NIH Image, we scored all 554 hair cells in these regions by stepping through the Z series and scoring each

hair cell as “type I” or “ type II” based on the following criteria (see Fig. 1). Type II hair cells had thicker and shorter necks than type I hair cells. The nuclei of type II hair cells were arranged in a near-monolayer near the lumen. The position of the type I hair cell nuclei varied with location. In extrastriolar regions, type I hair cell nuclei were arranged in a near-monolayer, deep to the type II hair cell nuclei and just above the supporting cell nuclei. In the striolar region, the nuclei of type I hair cells could also be closer to the lumen, particularly in hair cells within complex calyces. In utricles co-labeled for markers of neural fibers (neurofilament or β III tubulin), we noted that these features correlated well with the defining feature of these hair cell classes – the presence (type I) or absence (type II) of afferent nerve calyces.

Transmission electron microscopy

Temporal bones were isolated from adult CBA/CaJ mice, and a small hole was made in the temporal bone next to the oval window. Fixative (2% paraformaldehyde/3% glutaraldehyde in 0.1M sodium phosphate buffer, pH 7.4) was slowly injected into the labyrinth, and temporal bones were immersion-fixed overnight at 4°C. Utricles were isolated, and otoconia were removed. Utricles were post-fixed in 1% osmium tetroxide and embedded in Eponate 12 Kit with DMP-30 (Ted Pella, Inc). Ultrathin sections (85 nm) were collected onto grids and stained with 0.3% lead citrate in 0.1N sodium hydroxide and 5% uranyl acetate in 50% methanol. Sections were analyzed using a JEOL 1230 transmission electron microscope, equipped with an XR80 side-mount digital camera (Advanced Microscopy Techniques) and located in the Vision Imaging Core at the South Lake Union UW facility.

RESULTS

Identification of type I and type II hair cells in whole-mounts of adult mouse utricles

The goal of this study was to determine if type II vestibular hair cells in normal mature rodents have basolateral processes, similar to those we have observed in regenerated hair cells in mice (Golub et al., 2012). As a first step, we examined the basic features of type I and type II hair cells in whole-mount preparations of adult mouse utricles. Utricles from adult (42 day-old) CBA/CaJ mice were labeled with antibodies to the hair cell-specific cytoplasmic protein myosin VIIa (Hasson et al., 1997) and examined using confocal microscopy. As anticipated, anti-myosin VIIa antibodies labeled the cytoplasm of all hair cells in the macula, but they did not label any supporting cells or neural elements (Fig. 1A–D). Some myosin VII-positive cells resembled type I hair cells; they were flask-shaped and had a long and thin apical “neck” and a rounded cell body, with little cytoplasm surrounding the nucleus (Fig. 1C,D). Co-labeling with antibodies to parvalbumin, a marker of vestibular afferents (Demêmes et al., 1993; Fig. 1C,D), and other neural markers (βIII tubulin, 28kD calbindin, and 200kD neurofilament; not shown) indicated that the neck and cell body of such cells were wrapped by complete or partial afferent nerve calyces. In the striola (a specialized region in the center of the macula, Fig. 1E), many type I hair cells appeared to be wrapped almost entirely by nerve calyces, and their nuclei were located near the lumen (Fig. 1C). Other type I-like hair cells with nerve calyces had nuclei located deeper in the epithelium (Fig. 1C). In regions outside of the striola (extrastriolar regions, Fig. 1E), type I hair cell nuclei were located deep in the epithelium, just above the supporting cell nuclei. All

remaining myosin VIIa-labeled cells were type II-like and had a similar appearance, regardless of whether they were located in striolar or extrastriolar positions. Their apical portion was thicker (Fig. 1B) and their nucleus was located closer to the lumen (Fig. 1D) than type I hair cell nuclei. Further, type II hair cells lacked neural calyces (Fig. 1D). Similar observations were made with antibodies to myosin VI, another hair cell marker (data not shown). In contrast, antibodies to calretinin (calbindin2) labeled primarily hair cells with type II characteristics (data not shown), as described previously (Desai et al., 2005). We made similar observations in two other strains of adult mice (C57Bl/6J and Swiss Webster).

Using myosin VIIa labeling and morphological criteria (nuclear position and apical cell thickness) in CBA/CaJ mouse utricles, we determined that there were 1.17 (±0.35 S.D.) type I hair cells for every type II hair cell in randomly selected regions (striolar and extrastriolar). Similar measurements were made in other mouse studies (Kirkegaard and Nyengaard, 2005; Desai et al., 2005).

Type II-like hair cells in adult mouse utricles have basolateral processes

Most of the morphological features described above for type I and II hair cells in mammalian vestibular epithelia have been clearly defined in prior publications (e.g., Lysakowski and Goldberg, 1997). We identified two novel features of type II hair cells in adult CBA/CaJ mouse utricles that are illustrated in Fig. 2. Figure 2B1–4 shows confocal Z series images taken in the utricular macula, starting at the lumen and ending near the supporting cell nuclei. Positions of each image are indicated in Fig. 2A, which is a schematic section of the utricular macula. As described in Fig. 1, type II hair cells were readily distinguished by their expanded apical surface and nuclei closest to the lumen. By following these cells through Z series, we found that most type II hair cells had a short and narrow cytoplasmic constriction below the nucleus (Fig. 2A,B3,C). This feature, which we named a “waist”, was located at the same level as the type I hair cell nuclei. Below the waist, the type II hair cell cytoplasm expanded (Fig. 2B4). In some type II hair cells, this cytoplasmic expansion gave rise to one or more myosin VIIa-positive extensions that coursed laterally in the horizontal plane, parallel to the lumen (Fig. 2A,B4,C). These basolateral processes spread below the type I hair cell nuclei, near the level of the supporting cell nuclei. Although processes descended quite basally in the sensory epithelium (see Fig. 3F), we did not detect any processes that contacted the basal lamina. Basolateral processes were also immunoreactive for the cytoplasmic protein calretinin (Fig. 2E) and the transcription factor Sox2 (Fig. 2F1–G), two preferential markers of type II hair cells (Desai et al., 2005; Oesterle et al., 2008). Basolateral processes were not labeled by antibodies to either heavy weight (200 kD) neurofilament (Fig. 2H,I) or class III β tubulin (not shown), but they were immunoreactive for myosin VI, another cytoplasmic hair cell marker (not shown). These findings indicate that the basolateral processes belong to type II hair cells rather than neurons or type I hair cells. Fig. 2D summarizes the shape and molecular features of the type II hair cell processes described in this figure.

Further analysis with myosin VIIa immunolabeling in whole-mount preparations revealed that nearly every type II hair cell in the utricle had a cytoplasmic expansion below its waist (and deep to the type I hair cell nuclei). However, the shape and extent of this expansion

varied considerably. In approximately 20% of type II hair cells, the basal cytoplasm expanded into a simple bulbous shape (Fig. 3A,D1,E1). For 60% of type II hair cells, two or more processes extended laterally from the base for distances up to 4 hair cell widths and were sometimes branched (Fig. 3B,C,D3,E3). The remaining 20% of type II hair cells had intermediate phenotypes (e.g., shorter processes with no branches)(Fig. 3D2,E2). We detected no clear trends with respect to process orientation or a regional variation in process morphology.

Findings with confocal microscopy were confirmed by TEM analyses of transverse and horizontal sections (Fig. 3F,G). Hair cells or hair cell processes were easily distinguished from other cellular elements based on ultrastructural characteristics. Most notably, their polyribosome-rich cytoplasm (e.g., Fig. 3F inset, also see Figs. 7 and 8) clearly differentiated them from afferent or efferent neurites, which lack polyribosomes. Further, their cytoplasm was distinct from supporting cell cytoplasm, which had fewer polyribosomes and, in some regions of the cell body, many lysosome-like structures. Type II hair cells were differentiated from type I hair cells based on their lack of a calyx and their apically located nucleus. In transverse sections, we could identify type II hair cells with basal processes that nearly reached the basal lamina and had lateral branches (Fig. 3F). In horizontal or near-horizontal sections (taken parallel to the lumen and near the plane of the supporting cell nuclei), we saw processes with hair cell cytoplasm that extended laterally for several cell diameters (Fig. 3G). Based on three-dimensional reconstructions and transmission electron micrographs, we estimated that basolateral processes were typically between 0.50 and 2 μm thick.

Basolateral processes of type II hair cells are present in cristae and saccules of adult mice and are conserved in other rodents

To determine if type II hair cell processes are a unique feature of utricles in CBA/CaJ mice or are shared by other vestibular organs and rodents, we used myosin VIIa immunolabeling to assess type II hair cell morphologies in a variety of other whole-mount vestibular organs. Type II hair cells with basolateral processes were abundant in utricles from two other strains of mice (C57Bl/6J and Swiss Webster) at a range of ages (42–365 days)(data not shown). We also detected processes on type II hair cells in saccules (Fig. 4A) and lateral ampullae (not shown) of adult mice of all three strains (CBA/CaJ, C57Bl/6J, and Swiss Webster; an image from a CBA/CaJ mouse is shown in 4A). In addition, we examined three other types of rodents for evidence of type II hair cell processes. Using myosin VIIa immunolabeling, we found that type II hair cells in the utricles of adult rats (Fig. 4B), gerbils (Fig. 4C), and bats (Fig. 4D) also have pieces of cytoplasm that extend below their nuclei. In rats, we saw only minimal lateral extensions, despite similar fixation and labeling methods as for mice. In gerbils and bats, basal processes of some type II hair cells had pronounced lateral extensions, similar to mice.

Type II hair cells with extensive basolateral processes have mature properties

Basal processes have not been described in mature mammalian hair cells, but they have been associated with an immature hair cell status in non-mammals (e.g., Whitehead and Morest, 1985; Steyger et al., 1997; Stone and Rubel, 2000). To assess the maturity of type II hair

cells with processes in mice, we tested if they rapidly incorporate the styryl dye, FM1-43, a property that is associated with functional mechanoelectric transduction (MET) channels (Gale et al., 2001; Géléoc and Holt, 2003; Meyers et al., 2003). Utricles from adult Swiss Webster mice were explanted and immersed for 20 sec in 37°C FM1-43, rinsed, and maintained for 30 minutes at 37°C. Utricles were then fixed, labeled with antibodies to myosin VIIa, and imaged as whole-mounts. FM1-43 was readily detected in the apical and perinuclear regions of most myosin VIIa-positive cells, including type I and II hair cells (Fig. 5A,B). FM1-43 was also detected in some type II hair cell processes (Fig. 5C,D). FM1-43 did not accumulate in any other cell types in the preparation, including supporting cells. These findings show that type II hair cells with processes rapidly incorporate FM1-43 and therefore are likely to have functional MET channels.

Type II hair cells in mice appear to contact one another via basolateral processes

Additional observations suggest that the processes of many type II hair cells in adult mouse utricles contact one another and form a network amongst hair cells in a given region. Digital segmentation of selected myosin VIIa-labeled hair cells from adult CBA/CaJ mice revealed that some type II hair cells may contact at least three other type II hair cells (Fig. 6A1–A3; e.g., cell #4). The level of connectivity amongst type II hair cells was apparent in projection images of utricles labeled with antibodies to calretinin (Fig. 6B), a selective marker of type II hair cells. Potential sites of contact between type II hair cell processes were also evident in thick transverse sections through the utricular macula (Fig. 6C). In addition, type II processes appeared to contact afferent calyceal endings surrounding type I hair cells (Fig. 6D). Synaptic contact between the cell body of type II hair cells and the outer face of the calyx has been demonstrated before (e.g., Goldberg et al., 1990; Lysakowski and Goldberg, 1997; Ross, 1997). Here, we show that basolateral processes of type II hair cells may also contact the outer face of the calyx.

TEM enabled us to visualize sites of contact between the basolateral processes of nearby type II hair cells (Fig. 7). At some sites, the plasma membranes of the two processes were closely apposed, but no specializations were evident (Fig. 7A,B,C). At a few regions where processes were apposed, we noted increased electron density that could be indicative of a specialized form of contact between hair cells (Fig. 7B,D). In our investigations so far, we have not detected any concrete evidence for synapses or gap junctions between the processes of type II hair cells.

The basolateral processes of type II hair cells form ribbon synapses with vestibular afferents

To begin to address if basolateral processes of type II hair cells communicate with neural elements, we used immunofluorescence in adult mouse utricles to identify hair cell synapses with vestibular afferents. We labeled utricles from CBA/CaJ mice with antibodies to ctbp2 (C-terminal binding protein 2, or ribeye) to label pre-synaptic ribbons in hair cells (Schug et al., 2006; Uthaiah and Hudspeth, 2010) and myosin VIIa to label hair cell cytoplasm. Confocal microscopy revealed that, in type II hair cells, ctbp2 antibodies bound to numerous small round or oval structures characteristic of ribbon synapses at the levels of the waist (Fig. 8A2) and the basolateral processes (Fig. 8A3). However, very little ctpb2 labeling was

seen in type II hair cells at the level of the nucleus (Fig. 8A1). We also found that some ctbp2-positive structures in basolateral processes were closely apposed to thin neurofilament-positive structures resembling neurites (Fig. 8B). Next, we triple-labeled utricles from in adult CBA/CaJ mice with antibodies to ctbp2, glur2 (glutamate receptor 2, a post-synaptic protein), and myosin VIIa. This approach revealed close apposition of ctbp2 and glur2 at the level of the hair cell processes (Fig. 8C,D), confirming that type II processes are sites of many synapses with vestibular afferents.

To better examine synapses between basolateral processes and vestibular afferents, we used TEM. We determined that basolateral processes contain many classical synaptic ribbons: synaptic vesicles surrounding an electron-dense body (Fig. 8E–H). In many cases, a ribbon was opposed closely to an afferent nerve bouton that had clear dendritic features: neurofilaments, microtubules, and mitochondria (Fig. 8G,H). In addition, the plasma membrane of the afferent bouton near the ribbon was electron-dense, typical of a post-synaptic specialization (Fig. 8G,H). We also noted that some ribbons in type II hair cell basal (descending) processes were opposed to a nerve calyx of a type I cell (not shown), as has been described previously (e.g., Lysakowski and Goldberg, 1997).

The basolateral processes of type II hair cells receive synaptic inputs from vestibular efferents

Next, we tested the hypothesis that the basolateral processes of type II hair cells receive neural inputs from vestibular efferent fibers, which originate in the brainstem (reviewed in Highstein, 1991). We labeled utricles from CBA/CaJ mice with antibodies to choline acetyltransferase (chat), an acetylcholine synthetic enzyme that is present in vestibular efferents of mice and rats (Kong et al., 1994; 2002). Chat immunolabeling was seen in small club-shaped nerve endings that appeared to terminate on basolateral processes (Fig. 9A). TEM analysis confirmed the presence of efferent synapses on the basolateral processes (Fig. 9B). These synapses resembled those seen before in mammalian vestibular epithelia (e.g., Goldberg et al., 1990). The efferent ending was filled with regular small and clear synaptic vesicles (Fig. 9B inset), forming clusters near the pre-synaptic membrane. In some hair cells receiving efferent synapses, there was a membrane thickening and post-synaptic cistern (Fig. 9B, inset).

Type II hair cell processes develop post-natally

Vestibular hair cells differentiate during the late embryonic and early post-natal periods (e.g., Rüsch et al., 1998; Burns et al., 2012). We examined how type II hair cell processes develop by examining utricles from Swiss Webster mice at post-natal days (p) 7, 14, and 21. Utricles were immunolabeled to detect the type II hair cell marker calretinin and examined using confocal microscopy. At p7, some type II hair cells had cytoplasmic expansions below the waist (Fig. 10A), but no lateral extensions (processes) were evident. At p14, spreading of the basal cytoplasm had occurred in some type II hair cells, but very few lateral extensions were seen (Fig. 10B). At p21, many type II hair cells exhibited lateral extensions (Fig. 10C), some of which were branched. By p42 (adult), long and branched processes were detected in many type II hair cells (Fig. 10D). Similar general observations were observed with antibodies to myosin VIIa, a second marker of basolateral processes (not shown).

Using image processing software, we analyzed how the basolateral processes of type II hair cells change between p7 and p42 by measuring the mean surface area, volume, and perimeter boundary for several hair cells at p7, p14, p21 and p42 (see Materials and Methods for details). Grouped data were subjected to one-way analysis of variance. Although there was considerable variation in measurements across sampled regions at all of the ages we studied, all 3 parameters (surface area, volume, and perimeter boundary) were significantly increased over time ($p<0.0001$)(Fig. 10E–G). Post-hoc analyses with Bonferroni Multiple Comparison correction showed that: 1) process surface area was significantly different between all ages except between p21 and adult; 2) process volume was significantly different between all ages except between p14 and adult; and 3) perimeter boundary was significantly different between all time-points except between p7 and p14.

These findings demonstrate that type II hair cell processes undergo dynamic morphological transitions between p7 and p21, at which point many aspects of the murine vestibular epithelium have matured (e.g., Nordemar, 1983; Rüsch et al., 1998). At the later stages of development (between p21 and p42), there were only small adjustments in the surface area and volume, but the process perimeter continued to increase. These findings demonstrate that basolateral processes tend to extend and become thinner during the later stages of development. However, as defined in Fig. 3, considerable variation in process surface area, volume, and perimeter remains across the type II hair cell population in adult mice.

DISCUSSION

Body orientation and movement depend largely upon vestibular hair cells, which serve as gravity and motion detectors and relay information about head position and motion to various regions of the brain. Many morphological, physiological, and molecular features of both type I and II vestibular hair cells have been studied in mature and developing mammals (for a recent review, see Eatock and Songer, 2011). Here, we present the first account of a striking feature of mammalian type II hair cells: cytoplasmic processes that extend laterally from the basal-most portion of the hair cell. These basolateral processes course below type I hair cells and form contacts with vestibular nerves (afferents and efferents) and with other basolateral processes, constituting a network amongst type II hair cells. Although further analysis is required to define the nature of the type II hair cell coupling, these initial observations have important implications for many aspects of vestibular biology, including peripheral signal processing, cellular homeostasis, and hair cell regeneration.

Type II hair cells in rodents have large basolateral processes

The morphology of type II hair cells has been studied, with some of the best analyses conducted in the cristae of mature chinchilla (Lysakowski and Goldberg, 1997) and guinea pig (Wersäll, 1956). Using TEM to examine transverse sections, these studies showed that type II hair cells have a cylindrical, goblet, or dumbbell shape (i.e., a relatively large apical region, a narrow central region, and a large basal region). Here, we used immunofluorescence labeling and confocal microscopy to assess type II hair cell morphology in adult mice, gerbils, rats, and bats. Our analyses confirmed the dumbbell shape in some type II hair cells in all of these species. We also found that many type II hair

cells in mice, gerbils, and bats extend lateral cytoplasmic processes from their enlarged basal region. The basal processes course horizontally in the epithelial plane, passing under the type I hair cells and above the level of supporting cell nuclei. Basolateral processes can be thick (0.5 to 2 μm), long (up to 3 hair cell widths), and/or branched. In mice, these processes are readily detected using antibodies to myosin VI, myosin VIIa, or calretinin. TEM analysis confirmed that type II processes have long basolateral extensions and showed that the processes of some type II hair cells descend to a level very close to the basal lamina.

There are several plausible explanations for why basolateral processes have not been identified previously in mammalian type II hair cells. Most morphological analyses of vestibular tissue have been conducted in thin transverse sections. This type of preparation makes it difficult to identify basolateral processes, which course in and out of the plane of section. By contrast, inspection of immunofluorescently labeled hair cells in whole-mount organs or thicker sections using confocal microscopy enables visualization of the entire hair cell and therefore facilitates the detection of hair cell processes, which course laterally. Another reason why hair cell processes were not noted before could be that many hair cell biologists favor the use of perinatal vestibular organs for mammalian studies, and we found that hair cell processes are not elaborated until the third post-natal week, at least in mice.

Initial observations of type II basolateral processes were made in hair cells that had regenerated in adult mouse utricles after damage (Golub et al., 2012). Regenerated hair cells were multipolar in appearance, with multiple branched processes extending from the cell bodies. This unusual morphology initially suggested that the new hair cells had matured abnormally. However, our current findings demonstrate that multipolar basolateral processes of type II hair cell are normal in some adult mammals. The only major qualitative difference we detected so far between the basolateral processes seen in normal type II hair cells versus regenerated type II hair cells is that the regenerated cells' processes are more spindly. These findings do not rule out the possibility that regenerated type II hair cells in adult mice are abnormal. However, they demonstrate clearly that the normal morphology of mammalian type II hair cells has not been fully appreciated.

Using similar immunolabeling and imaging approaches, we were unable to identify basolateral processes in type II hair cells of adult rats. We are unsure why this result was obtained, but at this time we feel it is not definite that rats lack type II hair cell processes. Accordingly, it is important to perform additional comparative studies to determine if basolateral processes on type II vestibular hair cells are conserved across mammals.

Basolateral processes of type II hair cells are major sites of neural contacts

Using confocal and transmission electron microscopy, we found that type II processes in adult mouse utricles have abundant synapses with vestibular afferent boutons. The density of boutons varies across the type II hair cell body; we detected very few pre-synaptic ribbons at the perinuclear region of type II hair cells, but we found a higher density of ribbons at the waist (the constricted region below the nucleus) and the basolateral processes. Similarly, Lysakowski and Goldberg (1997) reported in the chinchilla crista that many ribbon synapses are located below the nucleus of type II hair cells. Using TEM, we determined that synapses between basolateral processes and afferent boutons have a classical form, with a pre-

synaptic ribbon and a post-synaptic density. Although the function of the basolateral processes is not clear at this time, the expanded surface areas they impart would enable higher numbers of synapses per hair cell, which could improve signal transmission from type II hair cells to vestibular afferents.

In rodents, efferent nerves derived from the brainstem synapse upon both type II hair cells and vestibular afferents. Using confocal and transmission electron microscopy, we found in adult mouse utricles that some efferent synapses are localized to the basolateral processes of type II hair cells and such synapses have a mature, classical form. This finding strongly suggests that type II hair cell activity is modulated by efferents at all levels, including at the level of the basolateral processes.

Basolateral processes of type II hair cells contact one another

Our most striking observation is that type II hair cells in mice, gerbils, and bats are in direct contact with other type II hair cells at the level of the basolateral processes. We confirmed contacts between the processes in adult mouse utricles in both horizontal and transverse sections using TEM. Although most of the process-to-process interconnections presented as simple membrane appositions, we noted increased electron density at the site of some contacts (Fig. 7B,D) that could be indicative of a more specialized form of contact. However, at this point, we do not understand the nature of the communication between processes.

To the best of our knowledge, contacts between mature type II hair cells in vertebrates have never been described. By contrast, evidence for electrical coupling between hair cells or similar mechanotransducers has been presented for invertebrates, including sea anenomes (Mire et al., 2000), mollusks (Detwiler and Alkon, 1973), and squid (Williamson, 1989). In sea anenomes, inhibition of gap junctions between hair cells alters mechanotransduction-dependent signals, suggesting that electrical coupling is functionally significant (Mire et al., 2000). In the mammalian retina, there are gap junctions between visual receptors (rods and cones)(e.g., DeVries et al., 2002; Hornstein et al., 2005). This coupling is hypothesized to pool receptor voltages before the first synapse, resulting in improved signal-to-noise ratios. No similar mechanism has been postulated to exist in the vestibular epithelium. Nonetheless, our future studies will seek evidence for electrical or chemical coupling between mammalian type II hair cells.

It is possible connections between type II hair cells are purely physical, linking the cells in a network. Somatic coupling could affect the mechanics of signal transduction, for instance, by integrating several hair cells with the overlying otoconia. It is also possible that type II hair cells communicate by ligand-receptor interactions that transduce signals important for homeostasis and/or maintenance. One intriguing idea is that direct communication between type II hair cells regulates their state of differentiation or their life cycle. Vestibular hair cells are continually renewed in mature birds and other non-mammalian vertebrates (e.g., Jørgensen and Mathiesen, 1988). Prior studies suggest that hair cells in adult mammalian vestibular organs may also undergo turnover, because immature-appearing hair cells have been detected in normal mature organs (Forge et al., 1993; Rubel et al., 1995; Lambert et al.,

1997; Kirkegaard and Jørgensen, 2000). Clearly, further studies are required to determine the precise roles of process-to-process contacts amongst type II hair cells.

Type II hair cells display a range of morphologies in adulthood

The type II hair cells of mature mice exhibit considerable variability with respect to the shape and extent of their basal cytoplasm. Some hair cells have a simple bulbous expansion below the waist with no lateral extensions, as previously described (Lysakowski and Goldberg, 1997). Additional hair cells have highly ramified processes that extend laterally from the bulbous expansion as far as 3–4 hair cell lengths, while still others have only one or two short stumpy processes. We were unable to detect a spatial pattern with respect to distribution of these morphological hair cell variants. Further, we do not understand the reason for such variability nor if it has a functional consequence. One possibility is that there are subtypes of type II hair cells in mature mammalian vestibular epithelia. Type II hair cells throughout the utricle exhibit systematic variability with respect to the orientation and architecture of their stereociliary bundle (e.g., Li et al., 2008), but other systematic differences in morphological, physiological, or molecular features of type II hair cells have not been defined. Alternatively, as discussed above, mammalian type II hair cells may undergo normal turnover similar to birds, and the various morphologies may reflect hair cells at distinct stages of differentiation. These important questions will be addressed in future studies.

Acknowledgments

Acknowledgment of Support

This work was supported by: NIH/NIDCD grants R01 DC003696 (JSS), R21 DC011630 (JSS), and P30 DC04661 (Communications Research Imaging Core); NIH/NEI grant P30 EY001730 (Vision Imaging Core); and a Virginia Merrill Bloedel Traveling Scholarship (to RP).

We are grateful to Linda Robinson for assistance with mouse husbandry and genotyping, Glen MacDonald for assistance with digital imaging, Connor Finkbeiner, a visiting high school student, for assistance with cell counting, and Patricia White (University of Rochester) for assistance with immunolabeling. We are grateful to Dale Cunningham, as well as Dan Possin and Ed Parker at the Core for Vision Research (UW), for assistance with transmission electron microscopy. We appreciate the assistance of Armin Seidl, Yuan Wang, Kimberly Miller, Allison Hixon, Edwin Rubel, and Ellen Covey (from the University of Washington) in providing temporal bones from gerbils, rats, and bats. We thank Liz Oesterle (UW), David Perkel (UW), Ed Rubel (UW), and Ruth Anne Eatock (Harvard Medical School) for helpful discussions and/or feedback on the manuscript.

LITERATURE CITED

Ackermann J, Ashton G, Lyons S, James D, Hornung JP, Jones N, Breitwieser W. Loss of ATF2 function leads to cranial motoneuron degeneration during embryonic mouse development. PLoS One. 2011; 6(4):e19090. [PubMed: 21533046]

Burns JC, On D, Baker W, Collado MS, Corwin JT. Over half the hair cells in the mouse utricle first appear after birth, with significant numbers originating from early postnatal mitotic production in peripheral and striolar growth zones. J Assoc Res Otolaryngol. 2012; 13(5):609–27. [PubMed: 22752453]

Cai T, Seymour ML, Zhang H, Pereira FA, Groves AK. Conditional deletion of Atoh1 reveals distinct critical periods for survival and function of hair cells in the organ of Corti. J Neurosci. 2013; 33(24):10110–22. [PubMed: 23761906]

Correia MJ, Lang DG. An electrophysiological comparison of solitary type I and type II vestibular hair cells. Neurosci Lett. 1990; 116(1–2):106–11. [PubMed: 2259440]

Cunningham LL, Cheng AG, Rubel EW. Caspase activation in hair cells of the mouse utricle exposed to neomycin. J Neurosci. 2002; 22(19):8532–40. [PubMed: 12351727]

Demêmes D, Eybalin M, Renard N. Cellular distribution of parvalbumin immunoreactivity in the peripheral vestibular system of three rodents. Cell Tissue Res. 1993; 274(3):487–92. [PubMed: 8293446]

Dechesne CJ, Winsky L, Kim HN, Goping G, Vu TD, Wenthold RJ, Jacobowitz DM. Identification and ultrastructural localization of a calretinin-like calcium-binding protein (protein 10) in the guinea pig and rat inner ear. Brain Res. 1991; 560(1–2):139–48. [PubMed: 1722130]

Del Rio T, Nishitani AM, Yu WM, Goodrich LV. In vivo analysis of lrig genes reveals redundant and independent functions in the inner ear. PLoS Genet. 2013; 9(9):e1003824. [PubMed: 24086156]

Detwiler PB, Alkon DL. Hair cell interactions in the statocyst of Hermissenda. J Gen Physiol. 1973; 62(5):618–42. [PubMed: 4356414]

Desai SS, Zeh C, Lysakowski A. Comparative morphology of rodent vestibular periphery. I. Saccular and utricular maculae. J Neurophysiol. 2005; 93(1):251–66. [PubMed: 15240767]

DeVries SH, Qi X, Smith R, Makous W, Sterling P. Electrical coupling between mammalian cones. Curr Biol. 2002; 12(22):1900–7. [PubMed: 12445382]

Eatock RA, Songer JE. Vestibular hair cells and afferents: two channels for head motion signals. Annu Rev Neurosci. 2011; 34:501–34. [PubMed: 21469959]

Fernández C, Baird RA, Goldberg JM. The vestibular nerve of the chinchilla. I. Peripheral innervation patterns in the horizontal and superior semicircular canals. J Neurophysiol. 1988; 60(1):167–81. [PubMed: 3404215]

Forge A, Li L, Corwin JT, Nevill G. Ultrastructural evidence for hair cell regeneration in the mammalian inner ear. Science. 1993; 259:1616–1619. [PubMed: 8456284]

Forge A, Li L, Nevill G. Hair cell recovery in the vestibular sensory epithelia of mature guinea pigs. J Comp Neurol. 1998; 397:69–88. [PubMed: 9671280]

Gale JE, Marcotti W, Kennedy HJ, Kros CJ, Richardson GP. FM1-43 dye behaves as a permeant blocker of the hair-cell mechanotransducer channel. J Neurosci. 2001; 21:7013–7025. [PubMed: 11549711]

Géléoc GS, Holt JR. Developmental acquisition of sensory transduction in hair cells of the mouse inner ear. Nat Neurosci. 2003; 6:1019–1020. [PubMed: 12973354]

Goldberg JM. Afferent diversity and the organization of central vestibular pathways. Exp Brain Res. 2000; 130(3):277–97. [PubMed: 10706428]

Goldberg JM, Lysakowski A, Fernández C. Morphophysiological and ultrastructural studies in the mammalian cristae ampullares. Hear Res. 1990; 49(1–3):89–102. [PubMed: 2292511]

Golub JS, Tong L, Nguyen Hume, CT, Palmiter RD, Rubel EW, Stone JS. Hair cell replacement in adult mouse utricles after targeted ablation of hair cells with diphtheria toxin. J Neuroscience. 2012; 32(43):15093–105.

Hasson T, Mooseker MS. Porcine myosin-VI: characterization of a new mammalian unconventional myosin. J Cell Biol. 1994; 127(2):425–40. [PubMed: 7929586]

Hasson T, Heintzelman MB, Santos-Sacchi J, Corey DP, Mooseker MS. Expression in cochlea and retina of myosin VIIa, the gene product defective in Usher syndrome type 1B. Proc Natl Acad Sci USA. 1995; 92(21):9815–9. [PubMed: 7568224]

Hasson T, Gillespie PG, Garcia JA, MacDonald RB, Zhao Y, Yee AG, Mooseker MS, Corey DP. Unconventional myosins in inner-ear sensory epithelia. J Cell Biol. 1997; 137(6):1287–307. [PubMed: 9182663]

Highstein SM. The central nervous system efferent control of the organs of balance and equilibrium. Neurosci Res. 1991; 12(1):13–30. [PubMed: 1660981]

Hornstein EP, Verweij J, Li PH, Schnapf JL. Gap-junctional coupling and absolute sensitivity of photoreceptors in macaque retina. J Neurosci. 2005; 25(48):11201–9. [PubMed: 16319320]

Jørgensen JM, Mathiesen C. The avian inner ear. Continuous production of hair cells in vestibular sensory organs, but not in the auditory papilla. Naturwissenschaften. 1988; 75(6):319–20. [PubMed: 3205314]

Kawamoto K, Izumikawa M, Beyer LA, Atkin GM, Raphael Y. Spontaneous hair cell regeneration in the mouse utricle following gentamicin ototoxicity. Hear Res. 2009; 247:17–26. [PubMed: 18809482]

Kirkegaard M, Jørgensen JM. Continuous hair cell turnover in the inner ear vestibular organs of a mammal, the Daubenton's bat (Myotis daubentonii). Naturwissenschaften. 2000; 87(2):83–6. [PubMed: 10663140]

Kirkegaard M, Nyengaard JR. Stereological study of post-natal development in the mouse utricular macula. J Comp Neurol. 2005; 492(2):132–4. [PubMed: 16196029]

Kong WJ, Egg G, Hussl B, Spoendlin H, Schrott-Fischer A. Localization of chat-like immunoreactivity in the vestibular end organs of the rat. Hear Res. 1994; 75:191–200. [PubMed: 8071146]

Kong WJ, Scholtz AW, Hussl B, Kammen-Jolly K, Schrott-Fischer A. Localization of efferent neurotransmitters in the inner ear of the homozygous Bronx waltzer mutant mouse. Hear Res. 2002; 167(1–2):136–55. [PubMed: 12117537]

Lambert PR, Gu R, Corwin JT. Analysis of small hair bundles in the utricles of mature guinea pigs. Am J Otol. 1997; 18(5):637–43. [PubMed: 9303162]

Lapeyre P, Guilhaume A, Cazals Y. Differences in hair bundles associated with type I and type II vestibular hair cells of the guinea pig saccule. Acta Otolaryngol. 1992; 112(4):635–42. [PubMed: 1442010]

Li A, Xue J, Peterson EH. Architecture of the mouse utricle: macular organization and hair bundle heights. J Neurophysiol. 2008; 99:718–733. [PubMed: 18046005]

Liberman LD, Wang H, Liberman MC. Opposing gradients of ribbon size and AMPA receptor expression underlie sensitivity differences among cochlear-nerve/hair-cell synapses. J Neurosci. 2011; 31(3):801–8. [PubMed: 21248103]

Longair MH, Baker DA, Armstrong JD. Simple neurite tracer: Open source software for reconstruction, visualization and analysis of neuronal processes. Bioinformatics. 2011; 27(17): 2453–4. [PubMed: 21727141]

Lysakowski A, Goldberg JM. A regional ultrastructural analysis of the cellular and synaptic architecture in the chinchilla cristae ampullares. J Comp Neurol. 1997; 389(3):419–43. [PubMed: 9414004]

Meyers JR, MacDonald RB, Duggan A, Lenzi D, Standaert DG, Corwin JT, Corey DP. Lighting up the senses: FM1-43 loading of sensory cells through nonselective ion channels. J Neurosci. 2003; 23(10):4054–65. [PubMed: 12764092]

Mire P, Nasse J, Venable-Thibodeaux S. Gap junctional communication in the vibration-sensitive response of sea anemones. Hear Res. 2000; 144(1–2):109–23. [PubMed: 10831870]

Nordemar H. Postnatal development of the vestibular sensory epithelium in the mouse. Acta Otolaryngol. 1983; 96(5–6):447–56. [PubMed: 6605657]

Oesterle EC, Campbell S, Taylor RR, Forge A, Hume CR. Sox2 and JAGGED1 expression in normal and drug-damaged adult mouse inner ear. J Assoc Res Otolaryngol. 2008; 9(1):65–89. [PubMed: 18157569]

Peterson EH. Are there parallel channels in the vestibular nerve? News Physiol Sci. 1998; 13:194–201. [PubMed: 11390788]

Peterson EH, Cotton JR, Grant JW. Structural variation in ciliary bundles of the posterior semicircular canal. Quantitative anatomy and computational analysis. Ann N Y Acad Sci. 1996; 781:85–102. [PubMed: 8694489]

Rennie KJ, Correia MJ. Potassium currents in mammalian and avian isolated type I semicircular canal hair cells. J Neurophysiol. 1994; 71(1):317–29. [PubMed: 8158233]

Ricci AJ, Rennie KJ, Correia MJ. The delayed rectifier, IKI, is the major conductance in type I vestibular hair cells across vestibular end organs. Pflugers Arch. 1996; 432(1):34–42. [PubMed: 8662265]

Ross MD. Morphological evidence for local microcircuits in rat vestibular maculae. J Comp Neurol. 1997; 379(3):333–46. [PubMed: 9067828]

Rubel EW, Dew LA, Roberson DW. Mammalian vestibular hair cell regeneration. Science. 1995; 267(5198):701–7. [PubMed: 7839150]

Rüsch A, Eatock RA. A delayed rectifier conductance in type I hair cells of the mouse utricle. J Neurophysiol. 1996; 76(2):995–1004. [PubMed: 8871214]

Rüsch A, Lysakowski A, Eatock RA. Post-natal development of type I and type II hair cells in the mouse utricle: acquisition of voltage-gated conductances and differentiated morphology. J Neurosci. 1998; 18:7487–7501. [PubMed: 9736667]

Sadakata T, Itakura M, Kozaki S, Sekine Y, Takahashi M, Furuichi T. Differential distributions of the Ca2+-dependent activator protein for secretion family proteins (CAPS2 and CAPS1) in the mouse brain. J Comp Neurol. 2006; 495(6):735–53. [PubMed: 16506193]

Sage C, Ventéo S, Jeromin A, Roder J, Dechesne CJ. Distribution of frequenin in the mouse inner ear during development, comparison with other calcium-binding proteins and synaptophysin. Hear Res. 2000; 150(1–2):70–82. [PubMed: 11077193]

Sans A, Dechesne CJ, Demêmes D. The mammalian otolithic receptors: a complex morphological and biochemical organization. Adv Otorhinolaryngol. 2001; 58:1–14. [PubMed: 11885550]

Sans N, Vissel B, Petralia RS, Wang YX, Chang K, Royle GA, Wang CY, O'Gorman S, Heinemann SF, Wenthold RJ. Aberrant formation of glutamate receptor complexes in hippocampal neurons of mice lacking the GluR2 AMPA receptor subunit. J Neurosci. 2003; 23(28):9367–73. [PubMed: 14561864]

Schindelin J, Arganda-Carreras I, Frise E, Kaynig V, Longair M, et al. Fiji: an open-source platform for biological-image analysis. Nature Methods. 2012; 9(7):676–682. [PubMed: 22743772]

Schug N, Braig C, Zimmermann U, Engel J, Winter H, Ruth P, Blin N, Pfister M, Kalbacher H, Knipper M. Differential expression of otoferlin in brain, vestibular system, immature and mature cochlea of the rat. Eur J Neurosci. 2006; 24(12):3372–80. [PubMed: 17229086]

Soni LE, Warren CM, Bucci C, Orten DJ, Hasson T. The unconventional myosin-VIIa associates with lysosomes. Cell Motil Cytoskeleton. 2005; 62(1):13–26. [PubMed: 16001398]

Sousa AD, Andrade LR, Salles FT, Pillai AM, Buttermore ED, Bhat MA, Kachar B. The septate junction protein caspr is required for structural support and retention of KCNQ4 at calyceal synapses of vestibular hair cells. J Neurosci. 2009; 29(10):3103–8. [PubMed: 19279247]

Steyger PS, Burton M, Hawkins JR, Schuff NR, Baird RA. Calbindin and parvalbumin are early markers of non-mitotically regenerating hair cells in the bullfrog vestibular otolith organs. Int J Dev Neurosci. 1997; 15(4–5):417–32. [PubMed: 9263023]

Stone JS, Rubel EW. Temporal, spatial, and morphologic features of hair cell regeneration in the avian basilar papilla. J Comp Neurol. 2000; 417(1):1–16. [PubMed: 10660884]

Uthaiah RC, Hudspeth AJ. Molecular anatomy of the hair cell's ribbon synapse. J Neurosci. 2010; 30(37):12387–99. [PubMed: 20844134]

Wersäll J. Studies on the structure and innervation of the sensory epithelium of the cristae ampulares in the guinea pig; a light and electron microscopic investigation. Acta Otolaryngol Suppl. 1956; 126:1–85. [PubMed: 13326368]

Whitehead MC, Morest DK. The development of innervation patterns in the avian cochlea. Neuroscience. 1985; 14(1):255–76. [PubMed: 3974881]

Williamson R. Electrical coupling between secondary hair cells in the statocyst of the squid Alloteuthis subulata. Brain Res. 1989; 486(1):67–72. [PubMed: 2541872]

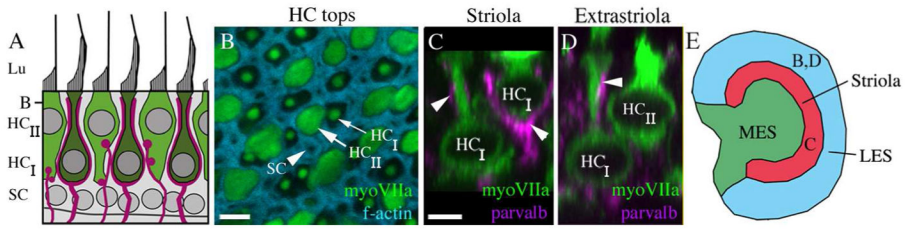

Figure 1.

Classical morphologies of type I and II hair cells in adult mouse utricles. A. A schematized transverse section of the extrastriolar region of the adult (6 week-old) CBA/CaJ mouse utricular macula, depicting the previously described features of type I hair cells (dark green cells, HC_I) and type II hair cells (light green cells, HC_{II}) and the positions of the hair cell and supporting cell (SC) nuclei. Magenta structures are vestibular afferents that either ensheath the type II hair cells or terminate in boutons on type II hair cells. The Z plane position of panel B is indicated. B. An image from the lateral extrastriolar region (see panel E) of a utricle labeled with antibodies to myosin VIIa (myoVIIa, green) and with phalloidin to detect filamentous actin (f-actin, cyan). This image is a horizontal (XY) confocal slice taken parallel to the lumenal surface of the epithelium at the level indicated in panel A. The thin arrow points to the neck of a type I hair cell, and the thick arrow points to the neck of a type II hair cell, both of which are myosin VIIa-positive. The arrowhead points to a supporting cell, which is f-actin-positive and myosin VIIa-negative. C. A transverse confocal slice (vertical re-slice) through two type I hair cells from the striolar region (see panel E) labeled with antibodies to myosin VIIa (green) and antibodies to parvalbumin (parvalb, magenta) to detect afferent nerves. The arrowheads point to calyceal elements on the type I hair cells. The orientation is similar to the schematic in panel A. D. A transverse confocal slice through a type I hair cell (HC_I) and a type II hair cell (HC_{II}) in the lateral extrastriolar region (see panel E) from a utricle labeled with anti-myosin VIIa and anti-parvalbumin. The arrowhead points to an afferent calyx on the neck of the type I hair cell. E. A drawing of the adult mouse utricle, showing the positions of the striola, lateral extrastriola (LES), and medial extrastriola (MES). The letters B,C, and D indicate the approximate sites of images shown in the corresponding panels. Lu = lumen, SC=supporting cell. Scale bar in B = 1.5 μm; scale bar in C = 4 μM (applies to C,D).

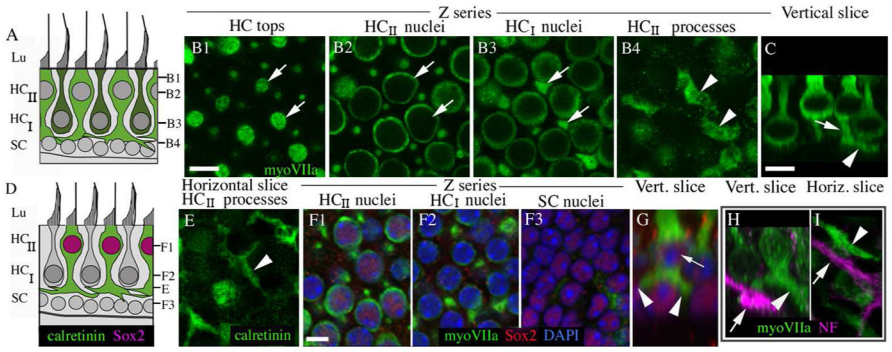

Figure 2.

Type II hair cells in adult mouse utricles have basolateral processes. All digital microscopy images were taken from the lateral extrastriolar region of utricles (see Fig. 1E for reference) from mice between 6 and 9 weeks of age. A. A schematized transverse section of the extrastriolar region of the adult CBA/CaJ mouse utricular macula, depicting the observed shapes of type I hair cells (dark green cells, HC_I) and type II hair cells (light green cells, HC_{II}) and the positions of the hair cell and supporting cell (SC) nuclei. The positions of the confocal slices shown in panels B1–4 are indicated. Panels B1–H show images from the lateral extrastriolar region of the adult mouse utricular macula. Panels B1–4 show horizontal confocal slices taken from one field of a utricle at successive depths in the epithelium (see A). The utricle was labeled with antibodies to myosin VIIa (myoVIIa, green) to detect hair cells. The arrows in each slice indicate two type II hair cells; a portion of their cell bodies is seen in each slice. C. A transverse confocal slice through the utricular macula, with an orientation similar to the schematic in A. The arrowhead points to a process, and the arrow points to the cell's waist. D. A drawing that illustrates the immunolabeling patterns for calretinin (green) and Sox2 (magenta) shown in panels E–G.). The letters E, F1, F2, and F3 indicate the approximate sites of images shown in the corresponding panels. E. Horizontal section through the basal layer showing type II hair cell processes (arrowhead) labeled with anti-calretinin (green). F1–F3. Horizontal slices through the same field in successive depths through the macula, immunolabeled for myosin VIIa (green) and Sox2 (red) and counter-labeled for DAPI (blue) to detect nuclei. G. A transverse slice showing a type II hair cell with a Sox2-positive nucleus (arrow) with two basolateral processes (arrowheads). H,I. Panels show the utricular macula immunolabeled for myosin VIIa (green) and 200kD neurofilament (NF, magenta) in transverse (H) and horizontal (I) confocal slices. Arrows in each panel point to NF-positive neural elements, and arrowheads point to myosin VIIa-positive type II hair cell processes. Scale bar in B1 = 6 μm (applies to B1–4); scale bar in C = 5 μm; and scale bar in F1 = 5 μm (applies to E,F1–I).

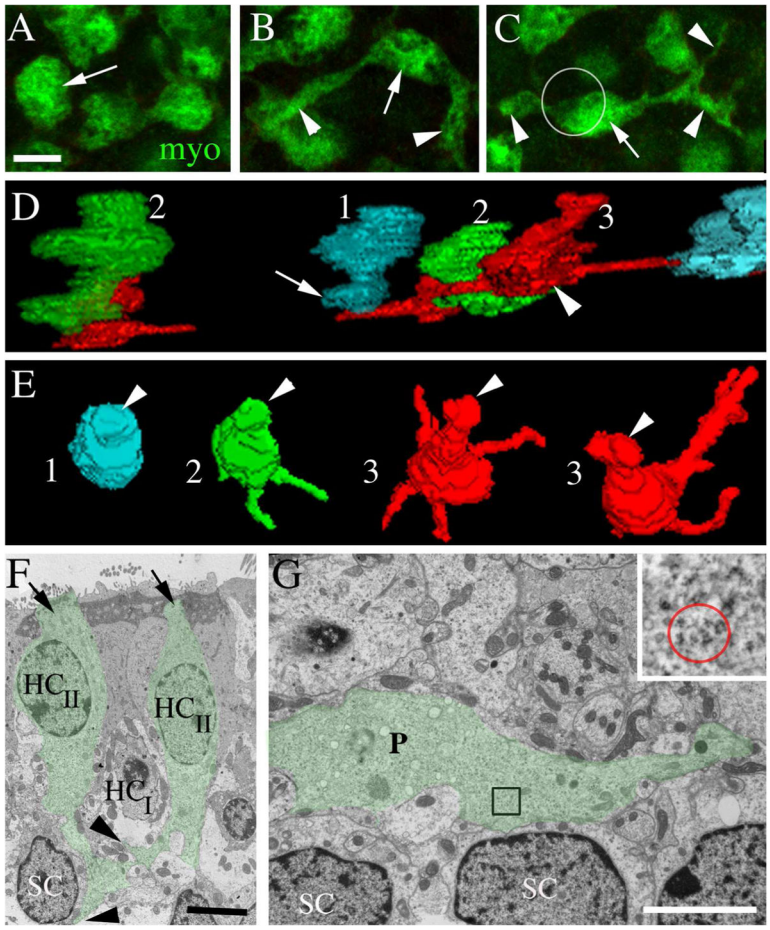

Figure 3.

Type II hair cell processes in adult mouse utricles have a range of morphologies. All images are from mice between 6 and 9 weeks of age. A–C are horizontal confocal slices showing the basal portion (i.e., the cytoplasm below the waist) of type II hair cells from the lateral extrastriolar region of an adult C57/Bl6 mouse utricle labeled with antibodies to myosin VIIa (myo, green). A. The arrow points to a type II hair cell in which the basal cytoplasm has a simple bulbous shape. B. The arrow points to the bulbous portion of a type II hair cell from which two long processes (arrowheads) emerge. C. The arrow points to the bulbous portion of a type II hair cell, and arrowheads point to its processes. The circle indicates the approximate location and size of the cell body (located in a more apical plane) relative to the basal portion. D,E. 3-D reconstructions of the basal portions of calretinin-labeled type II hair cells from different slices of the lateral extrastriolar region of a Swiss Webster mouse utricle. D = view from the side of the cell. E = ¾ view from the top of the cell. 1 (cyan) = hair cell with a simple bulbous basal portion. 2 (green) = hair cell with 1–2 basolateral processes. 3 (red) = hair cell with 3 or more basolateral processes. Some processes are obscured from view. F,G are ultrathin TEM sections through the extrastriolar region of an adult CBA/CaJ mouse utricle. F. Transverse section showing two type II hair cells (HC_{II}) with basal processes (green tint, arrows). The type II hair cell on the right has a lateral extension (upper arrowhead) emanating from its basal process and passing under a type I

hair cell (HC_I). The type II hair cell on the left has a foot process (lower arrowhead) that descends close to a supporting cell nucleus (SC). G. Horizontal section at the level near the type I hair cell and supporting cell nuclear layers showing a type II hair cell process (P, green tint) extending laterally near supporting cell nuclei (SC). G, inset. The red circle encompasses polyribosomes in the type II hair cell process at the position indicated in the boxed region in G. Scale bars: A = 5 μm (applies to A–C); F = 4 μm; and G = 4 μm.

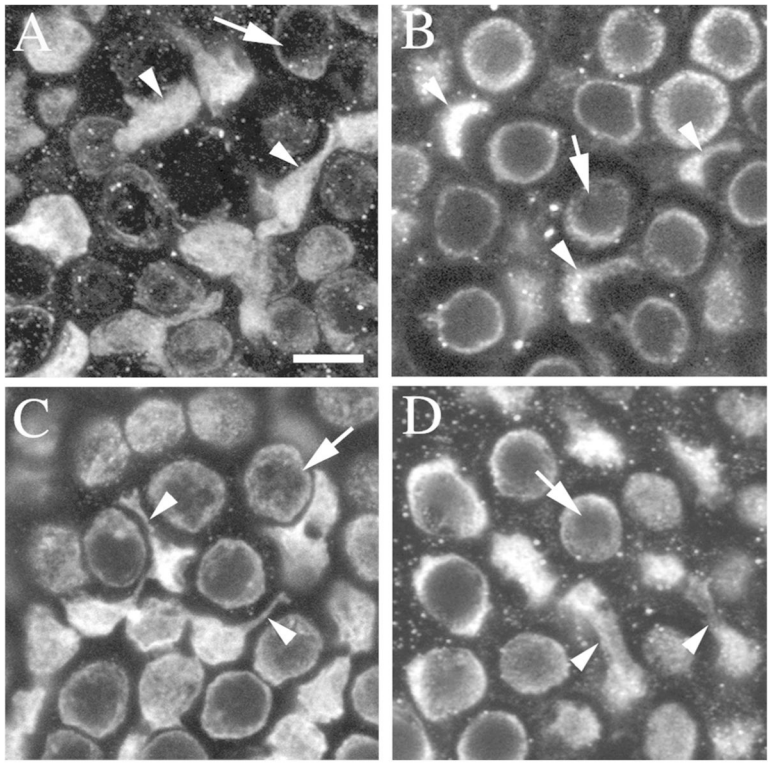

Figure 4.

Type II hair cells with processes are also present in the saccule and lateral ampulla of adult mice, gerbils, and bats. All images are horizontal confocal slices of various sensory epithelia from mature rodents, showing myosin VIIa immunolabeling and focused on the layer at or just under the type I hair cell nuclei. Arrowheads point to type II hair cell processes and arrows point to type I hair cell bodies. A. The lateral extrastriolar region of a 6 week-old CBA/CaJ mouse saccular macula. B. The lateral extrastriolar region of a utricle from a young, sexually mature rat (~40 days of age). C. The extrastriolar region of a sexually mature gerbil utricular macula. D. The extrastriolar region of a utricular macula from an adult bat (> 56 days of age). Scale bar in A = 5 μm (applies to A–D).

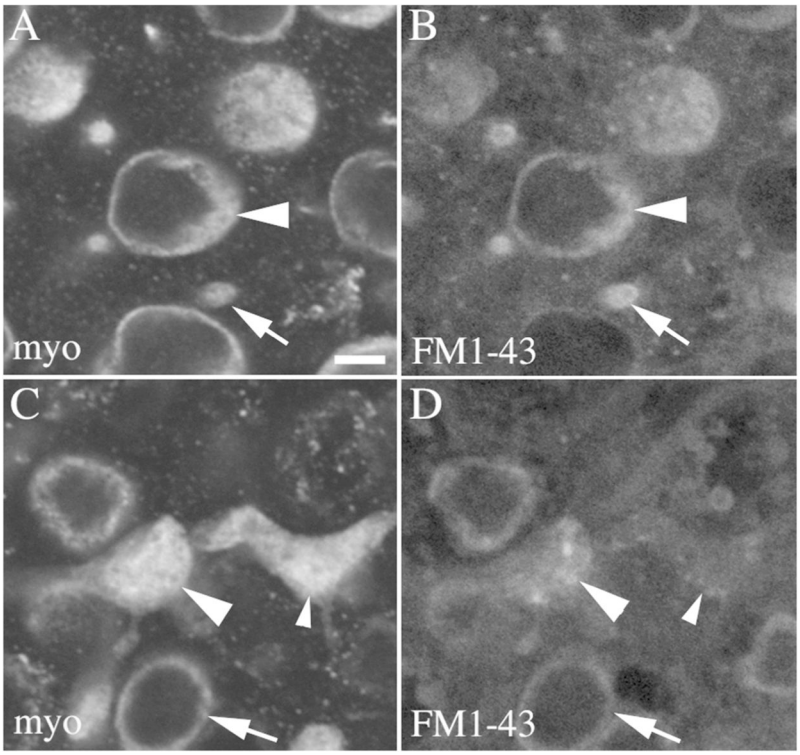

Figure 5.

Type II hair cells with basolateral processes utricles rapidly incorporate FM1-43. All panels show horizontal confocal slices from a 6 week-old Swiss Webster mouse utricle that was exposed for 20 seconds to FM1-43, rinsed and maintained in culture 30 minutes, then fixed and labeled for myosin VIIa and DAPI. Panels A,B show cells from the lateral extrastriolar region in a slice through the type II hair cell nuclei. Panel A shows myosin VIIa immunolabeling and panel B shows FM1-43 from the same field. Arrowheads point a type II hair cell body, and arrows point to the top of a type I hair cell. Panels C,D show the same field as A,B in a slice through type II hair cell processes. Panel C shows myosin VIIa immunolabeling, and panel D shows FM1-43 from the same field. The large arrowhead points to a basolateral process with substantial FM1-43 present, and the small arrowhead points to a basolateral process with only a little FM1-43 present. The arrow points to a type I HC with FM1-43 label in the perinuclear cytoplasm. Scale bar in A = 2 μm (applies to A–D).

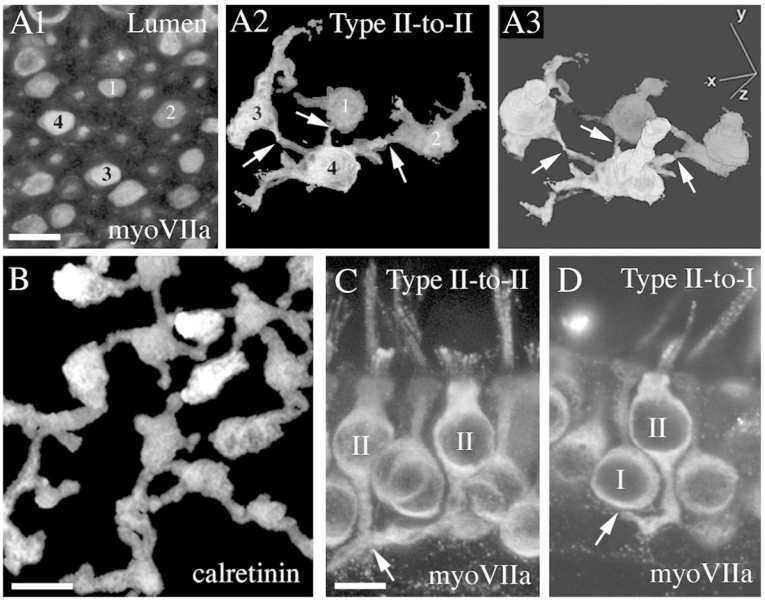

Figure 6.

The basolateral processes of nearby type II hair cells directly contact one another. All images are from mice between 6 and 9 weeks of age. A1–A3. Four myosin VIIa-labeled type II hair cells (numbered 1–4 in A1 and A2) were chosen for segmentation. A1 shows these cells in a horizontal slice near the lumenal surface of an adult CBA/CaJ mouse utricle (immunolabeled for myosin VIIa). The reconstruction shown in A2 is focused at the level of the hair cell processes. The reconstruction in A3 is a three-dimensional (3D) rendering of the whole cells. Arrows in A2 and A3 indicate possible points of contact. B. An image from an adult mouse (CBA/CaJ) utricle immunolabeled for calretinin to detect type II hair cells. This is a horizontal brightest point projection of horizontal slices taken from the hair cell waist to the basal lamina, revealing the shapes and possible connections of the basolateral processes of type II hair cells. C. Transverse vibratome section labeled for myosin VIIa showing a possible connection (arrow) between two type II hair cells (II). D. Transverse vibratome section labeled for myosin VIIa showing a possible connection (arrow) between one type II hair cell (II) and an afferent calyx surrounding a type I hair cell (I). Scale bars: A1 = 5 μm (applies to A1–A3); B = 5 μm; C = 5 μm (applies to C,D).

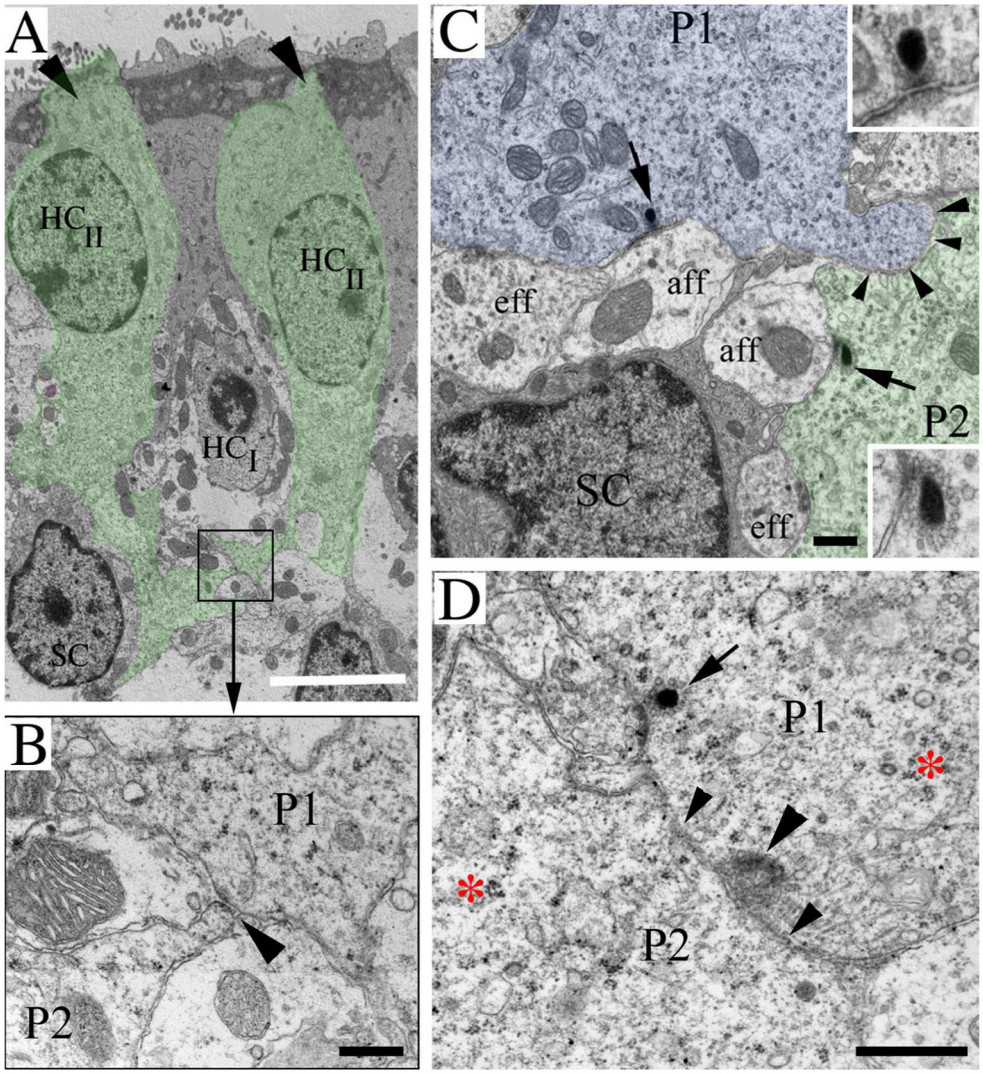

Figure 7.

Basolateral processes contact one another. All panels show ultrathin sections through utricles from normal CBA/CaJ mice between 6 and 9 weeks of age. A. A transverse section of two type II hair cells (HC_{II})(already shown in Fig. 3F) to illustrate the position of process-to-process contacts. The two type II hair cells are tinted green and indicated with arrows (at their tops); they surround a type I hair cell (HC_I). The boxed area shows a site of contact between two basolateral processes that is shown at higher magnification in panel B. B. Two processes, P1 and P2, have a point of contact (arrowhead). See panel A for position of this contact within the sensory epithelium. C. A horizontal section through the region near the supporting cell nuclei. The arrows point to ribbon synapses in type II hair cell processes (P1, tinted blue, and P2, tinted green) whose plasma membranes are closely apposed (arrowheads). Each ribbon synapse is shown at higher magnification in an inset. D. The contact site (small arrowheads) between two type II processes (P1 and P2) is shown. The large arrowhead points to a site of increased electron density in P1, next to its site of contact with P2. The arrow points to a ribbon synapse in P1. The higher magnification in panels B–

D provides evidence that the cytoplasm of the processes is full of polyribosomes, a hallmark of hair cells. An example of a cluster of polyribosomes is shown in D, to the right of the red asterisk in P2 and around the red asterisk in P1. SC = supporting cell nucleus; eff = efferent fiber; aff = afferent fiber. Scale bars: A = 5 μm; B, C, D = 500 nm.

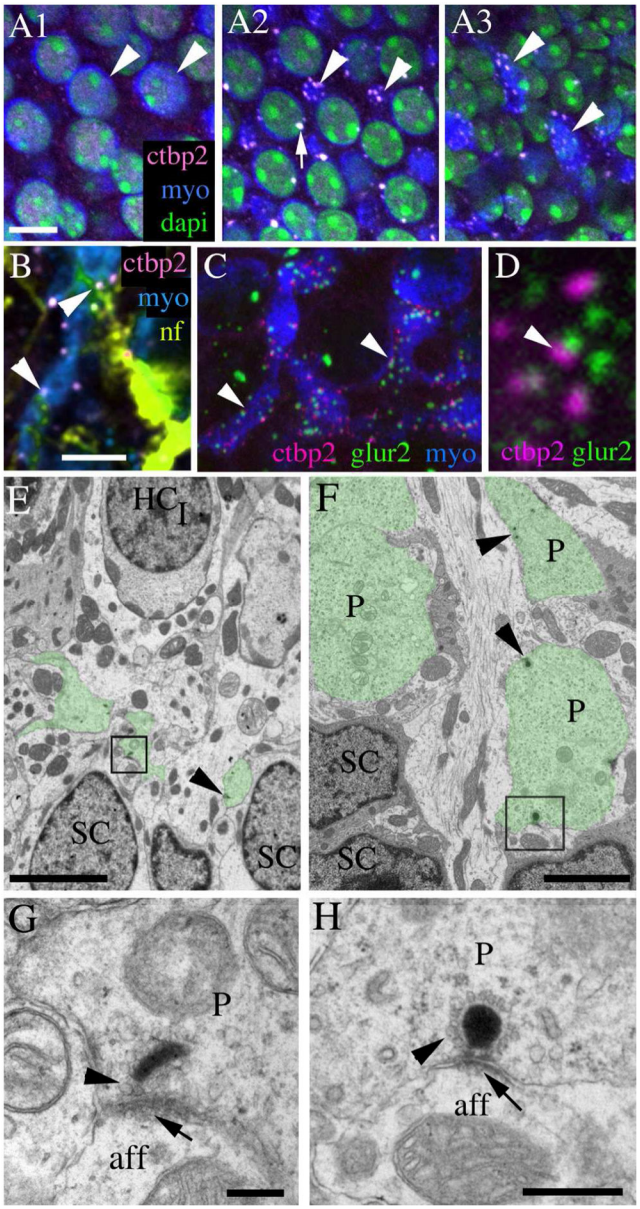

Figure 8.

Basolateral processes of type II hair cells form ribbon synapses with vestibular afferents. All images in this panel are derived from CBA/CaJ mice between 6 and 9 weeks of age. A1–A3. Confocal horizontal slices from a Z series showing the same field of a utricle labeled for myosin VIIa (blue), ctbp2 (pink), and dapi (green), focused on type II hair cell nuclei (A1), type I hair cell nuclei and type II hair cell "waists" (A2), or type II hair cell processes (A3). Arrowheads point to the same type II hair cells in all fields. Arrow in A2 indicates ctbp2 labeling in a type I hair cell. B. A horizontal slice through a utricle labeled for myosin VIIa (blue), ctbp2 (pink), and 200 kD neurofilament (nf, yellow-green). Arrowheads point to ctbp2 labeling in a type II hair cell basolateral process that is close association with neurofilament-labeled processes. C,D. Confocal horizontal slices through type II hair cell processes in a utricle labeled for myosin VIIa (blue), ctbp2 (majenta), and glur2 (green).

Arrowheads in C point to sites of co-labeling for ctbp2 and glur2. D shows this co-labeling at a higher magnification. EH. Ultrathin sections. E. A transverse section showing segments of basolateral processes (green tint) coursing under a type I HC (HC_I) and over supporting cell (SC) nuclei. The boxed area contains a synaptic ribbon that is shown at higher magnification in G. F. A horizontal section from a second utricle, taken near the supporting cell (SC) nuclei, shows segments of basolateral processes (P, green tint). The boxed area contains a synaptic ribbon that is shown at higher magnification in H. Arrowheads in F indicate positions of additional synaptic ribbons. G,H. Arrowheads point to vesicles around the electron dense region of the ribbon in the basolateral process that is opposed to an afferent (aff) bouton. Arrows point to the post-synaptic density in the afferent. Scale bars: A1 = 5 μm (applies to A1–A3): B = 5 μm (applies to B,C); E = 4 μm; F = 2 μm; G = 200 nm; H = 500 nm.

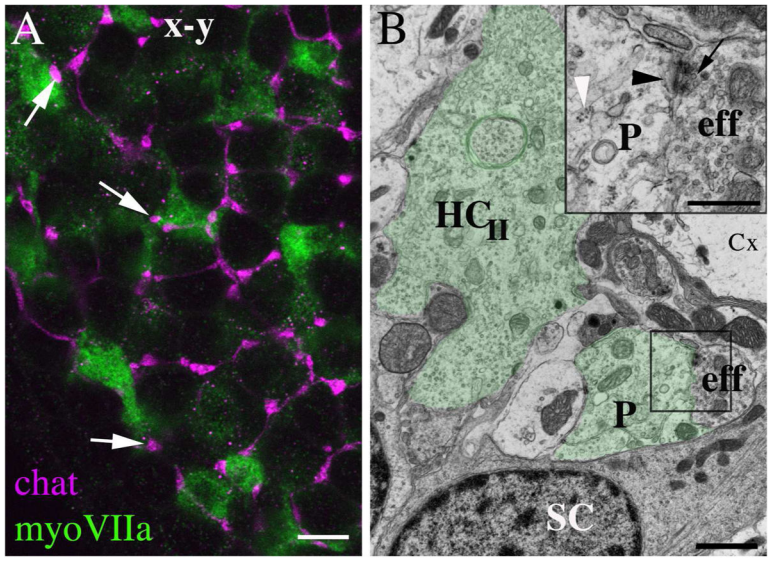

Figure 9.

Basolateral processes of type II hair cells receive synaptic inputs from vestibular efferents. A. A horizontal confocal slice through the basolateral processes of type II hair cells in a 6 week-old CBA/CaJ mouse utricle labeled for myosin VIIa (green) and choline acetyl transferase (chat, magenta). Arrows point to three apparent sites of contact between efferent endings and basolateral processes. B. An ultrathin transverse section through a utricle from a 9 week-old CBA/CaJ mouse. The basolateral processes (P) of a type II hair cell (HC_{II}) of a type II hair cell are tinted green. The box indicates the site of an efferent nerve element (eff) that synapses on the process; this site is shown at higher magnification in the inset on the upper right. In the inset, the white arrowhead points to polyribosomes in the hair cell process, the black arrowhead points to the post-synaptic cistern in the hair cell, and the black arrow points to the pre-synaptic vesicles in the efferent nerve element (eff). SC = supporting cell, Cx = calyx of a type I hair cell. Scale bars: A = 4 μm; B = 2 μm; inset B = 500 nm.

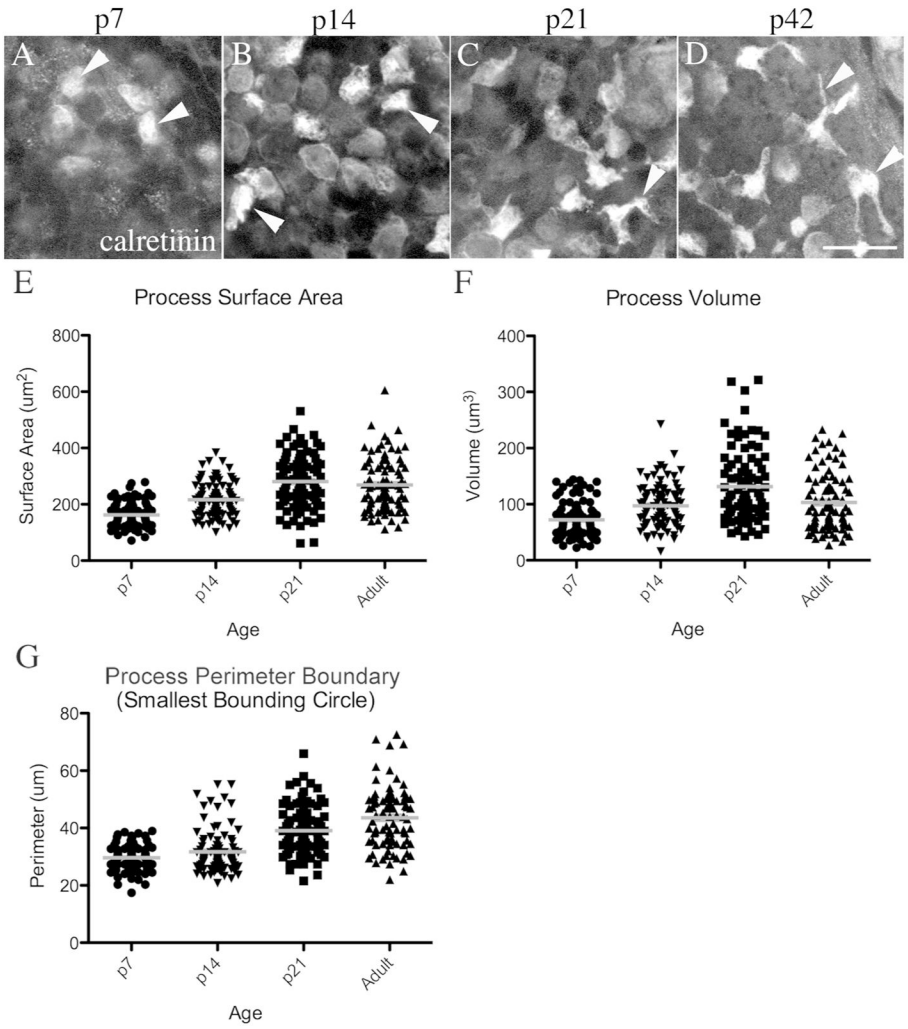

Figure 10.

Type II hair cell processes develop postnatally. A–D. Confocal horizontal slices of calretinin-labeled adult mouse utricles, focused on the epithelial layer where the type II hair cell processes are seen in adults (between the type I hair cell bodies and the supporting cell nuclei). The arrowheads point to examples of calretinin-labeled type II hair cell cytoplasm in this layer. E–G. Graphs show the distribution of measurements for process surface areas (E), process volume (F), and process perimeter boundary (G). Each point represents an individual cell, and the gray line represents the mean for each group of cells. Scale bar in D = 10 μm (applies to A–D).

J Comp Neurol. Author manuscript; available in PMC 2015 December 01.

Table 1

Antigen	Source and type of antibody	Immunogen	Specificity Controls	Dilutio
Myosin VI	Proteus Biosciences Cat# 25-6791 Rabbit polyclonal RRID:AB_10013626	Amino acids 1049–1254 of porcine myosin VI	Validated by immunoblot (Hasson and Mooseker, 1994). Shows expected pattern of mouse hair cell labeling, as defined (Hasson et al., 1997).	1:1000
Myosin VIIa	Proteus Biosciences Cat# 25-6790 Rabbit polyclonal RRID: AB_10015251	Amino acids 877–1075 of human myosin VIIa	Validated by immunoblot (Hasson et al., 1995). Shows expected pattern of mouse hair cell labeling, as defined (e.g., Hasson et al., 1997).	1:100
Myosin VIIa	Developmental Studies Hybridoma Bank Cat# 138-1 Mouse polyclonal RRID: AB_2282417	Amino acids 927–1203 of human myosin VIIa	Validated by immunoblot (Soni et al., 2005). Shows expected pattern of mouse hair cell labeling, as defined by Hasson et al. (1997) and Cai et al. (2013).	1:20
Calretinin	Millipore Cat# AB5054 Rabbit polyclonal RRID: AB_2068506	Recombinant rat calretinin (homologous to mouse)	Validated by immunoblot (manufacturer). Shows expected pattern of mouse hair cell labeling, as defined by Desai et al. (2005).	1:100
Calbindin	Millipore Cat# AB1778 Rabbit polyclonal RRID: AB_2068336	Recombinant mouse calretinin (28kD)	Validated by immunoblot (Sadakata et al., 2006). Showed expected pattern of mouse hair cell labeling, as defined by Cunningham et al. (2002) and Oesterle et al. (2008).	1:200
Parvalbumin	Sigma-Aldrich Cat# P3088 Mouse monoclonal RRID: AB_477329	Frog muscle parvalbumin	Validated by immunoblot (manufacturer). Shows expected pattern of mouse hair cell labeling, as defined in Sage et al. (2000).	1:200
Neurofilament	Millipore Cat# AB5539 Chicken polyclonal RRID: AB_177520	Purified bovine heavy-weight neuro-filament	Validated by immunoblot (manufacturer). Shows expected pattern of labeling of mouse inner ear nerve fibers, as defined by Goodrich et al. (2013).	1:1000
βIII tubulin	Covance Cat# MRB-435P Rabbit polyclonal RRID: AB_10175616	Rat brain microtubules	Validated by immunoblot (manufacturer). Shows expected pattern of labeling of mouse inner ear nerve fibers, as defined by Sousa et al. (2009).	1:200
GluR2	Millipore Cat# MAB397 Mouse monoclonal IgG2a RRID: AB_2113875	Recombinant fusion protein, amino acids 175–430	Validated by immunoblot (Sans et al., 2003). Shows expected pattern of labeling of mouse inner ear synapses, as defined by Liberman et al. (2011).	1:200
Ctbp2	BD Biosciences Cat# 612044 Mouse monoclonal IgG1 RRID: AB_399431	Amino acids 361–445 of mouse Ctbp2	Validated by immunoblot (manufacturer). Shows expected pattern of labeling of mouse inner ear synapses, as defined by Schug et al. (2006).	1:100
Sox2	Santa Cruz Bioche Cat# 17320 Goat polyclonal RRID: AB_2286684	Peptides from human Sox2 C-terminus	Validated by immunoblot (manufacturer). Shows expected pattern of mouse hair cell labeling, as defined by Oesterle et al. (2008).	1:100
Choline acetyl transferase	Millipore Cat# AB144P Goat polyclonal RRID: AB_2079751	Human placental choline acetyl transferase	Validated by immunoblot (manufacturer). Shows expected pattern of labeling in mammalian utricle (Kong et al., 1994).	1:200